Lingyan Zhang*, Yunxue Jin, Xitong Wang, Jie Cai* and Qingfeng Guan

# Surface Alloys of 0.45 C Carbon Steel Produced by High Current Pulsed Electron Beam

https://doi.org/10.1515/htmp-2018-0065
Received April 10, 2018; accepted September 11, 2018

**Abstract:** The chromium was deposited on the surface of 0.45 C medium carbon steel by high current pulsed electron beam (HCPEB) alloying treatment to obtain a high quality alloying layer. The microstructure of the alloying layer was studied by X-ray diffraction, optical microscopy, scanning electron microscopy (SEM), and transmission electron microscopy. The hardness of the surface was measured by Vickers durometer. The corrosion resistance of samples before and after HCPEB irradiation was also measured by an electrochemical workstation. The results showed that the alloying layer with a dept of about 4–9 μm on the surface was formed after HCPEB alloying treatment. TEM results revealed that the Cr element is dissolved on the surface and alloyed with C element in the substrate to form $Cr_{23}C_6$ enhanced particles. The microhardness and corrosion resistance of the medium carbon steel subjected to a HCPEB alloying processing were remarkably improved compared with the original one.

**Keywords:** HCPEB, surface alloying, microstructure, microhardness, corrosion resistance

## Introduction

The 0.45 C medium carbon steel is one of the most used structural materials, such as shafts and gears in the manufacture, some of the main force components and steel structures [1–3]. However, its hardness and corrosion resistance are relatively poor. In many cases, it is often difficult to meet the requirements of practical use, in particular the abrasion and corrosion resistance, which limits its applications [4, 5]. Surface alloying technology used on the steel surface to obtain a desired alloying layer is an effective method to improve the surface properties [6–8]. Basically, this technology involves interactions between a solvent (substrate) and a solute (alloying elements) when the alloying elements are uniformly distributed in the alloying layer. Therefore, significant improvements in the surface hardness, strength, and corrosion resistance can be achieved [9, 10]. Furthermore, the resistance of thermal fatigue can be increased, and the service life of the workpiece can be improved [11], as well. Nowadays, there are several kinds of surface alloying technologies that are widely used, such as double glow plasma surface alloying technology, evaporative pattern casting technology, laser beam surface alloying, and ion beam implantation [12–16]. However, these methods have some disadvantages, such as high cost, complicated operation, long cycle, and low efficiency. For instance, the laser beam results in the coarse microstructure with relative long duration and the irradiated surface is easy to oxidize in a non-vacuum environment [17, 18].

High current pulsed electron beam (HCPEB) is a new type of surface modification technology [19–21]. During the instantaneous process of HCPEB bombardment, the higher energy ($10^7$–$10^9$ W/cm$^2$) acts on the surface of the material in a very short time (several microseconds), resulting in extremely rapid heating, cooling, melting, and even evaporation, followed by a rapid solidification. As a result, the formation of a dense remelted layer can be obtained. Many researchers focus on the change of mechanical properties of the materials after HCPEB treatment and the thermo-mechanical coupling mechanism involved in the materials surface modification by HCPEB irradiation [22–24]. However, the surface alloying on the medium carbon steel by HCPEB treatment is still occasionally applied. The HCPEB technology has a huge potential in surface alloying and unique advantages due to the local high energy density, instantaneous heating-cooling effect, and specific modified characteristics [25]. The substrate and coating can be simultaneously melted resulting in their combination at the interface, which can significantly improve the performance of materials.

***Corresponding authors: Lingyan Zhang,** The Atomic, Molecular & Materials Physics Group, School of Science, Nanjing University of Science and Technology, Nanjing 210094, P. R. China,
E-mail: zhanglingyan1115@hotmail.com
**Jie Cai,** Institute of Advanced Manufacturing and Modern Equipment Technology, Jiangsu University, Zhenjiang 212013, China,
E-mail: caijie@ujs.edu.cn
**Yunxue Jin,** School of Materials Science and Engineering, Jiangsu University of Science and Technology, Zhenjiang 212013, China,
E-mail: 1270523067@qq.com
**Xitong Wang:** E-mail: qwertyasdfg@vip.qq.com, **Qingfeng Guan:** E-mail: guanqf@ujs.edu.cn, School of Materials Science and Engineering, Jiangsu University, Zhenjiang 212013, China

In this paper, 0.45 C medium carbon steel was used as an experimental substrate in the annealed state. Chromium (Cr) powder was precoated on the surface. The surface alloying of medium carbon steel was carried out by HCPEB irradiation. The microstructural characterization and performance test were investigated, and the alloying mechanism after HCPEB treatment was studied in detail.

## Materials and characterization techniques

The chemical composition of 0.45 C medium carbon steel used in the current investigation is 0.42–0.50 C wt %, 0.17–0.37 Si wt. %, 0.5–0.80 Mn wt. %, ≤ 0.035 P wt. %, ≤ 0.035 S wt. %, ≤ 0.25 Ni wt. %, ≤ 0.25 Cr wt. %, ≤ 0.25 Cu wt. %, and the balance Fe. The samples were cut into $10 \times 10 \times 10\,mm^3$ by wire electrical discharge machining. Before testing, the annealing process was carried out in a high temperature furnace, as follows. The sample was heated at 500 °C, then hold for 4 h, and finally cooled at 25 °C. The sample surface was grounded by using metallographic sandpapers and polished by diamond paste, and then washed with anhydrous ethanol. Cr powder (99.9 %, 30–40 μm particle size) was selected as the alloying material. A slurry was obtained by mixing 10 g Cr powder with an organic binder (100 mL, nitrocellulose lacquer : solvent = 1 : 2) and deposited on the polished surface with a thickness of about 0.05–0.1 mm by using a spraying gun. After drying, the polished surfaces of samples were irradiated using HOPE-I type source at room temperature. The irradiation was performed under vacuum of $10^{-5}$ torr, and using an electron energy of 27 keV, an energy density of $4\,J/cm^2$, a target distance of 150 mm, a current pulse duration of 1.5 μs, and an irradiated pulse number of 10, 20, and 30.

X-ray diffraction (XRD) with CuKα radiation was used for phase identification on a RigakuD/max-2500/pc X-ray diffractometer. The microstructural evolution was carefully analyzed by using LEICA DM-2500M optical microscope, JEOL JSM-7100F scanning electron microscope (SEM), and JEOL-2100 transmission electron microscope (TEM).

Microhardness was measured by a HVS-1000 device. To ensure the reliability of the measurements, five test points were installed in each sample. The electrochemical corrosion was measured using a Bio-Logic VMP2 electrochemical workstation with saturated calomel electrode as a reference electrode and platinum sheet as a counter electrode. The electrolyte was a 3.5 wt. % NaCl water solution. The cyclic polarization was done with a sweep rate of 0.333 mV/s. The tested specimen was exposed to the solution with an area of $1\,cm^2$, and the rest was sealed by vulcanized silicone rubber.

## Results and discussion

### XRD analysis

Figure 1 shows the XRD patterns of the samples before and after HCPEB alloying treatment. It can be seen that the original sample with no Cr powder was composed mainly of ferrite (α-Fe) phase. After HCPEB treatment, the peaks of martensite and austenite were detected, which indicated that the phase transformation occurred due to the thermostress coupling effect induced by HCPEB irradiation. Besides, compared to the initial one, the diffraction peak of austenite (γ-Fe) appeared on the irradiated surface, and

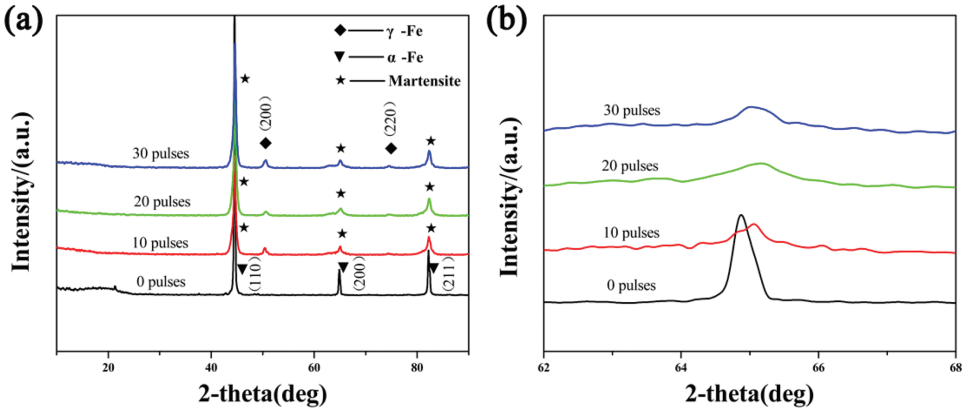


**Figure 1:** XRD analysis of medium carbon steel before and after HCPEB alloying. (a) XRD patterns, (b) enlarged view of the (200) diffraction peak.

the corresponding diffraction intensity was gradually increased with the increasing of the HCPEB pulses. This result indicates that the content of $\gamma$-Fe phase was increased, and Cr element has been dissolved into the substrate to form a solid solution. The width of diffraction peaks shows a remarkable broadening in comparison with the untreated one in Figure 1(b), which could result from the refined grain size caused by HCPEB irradiation. Previous reports have shown that HCPEB irradiation can induce a rapid remelting of the metal surface, as well as a the formation of a high number of nucleation sites, which have no enough time to grow during the next rapid cooling process [26]. Therefore, ultrafine crystals are developed on the metal surface, which are reflected by very broad and less intense diffraction peaks.

## Morphology of the surface and cross section

Figure 2(a) shows the metallographic structure of the initial sample. It can be seen that, before HCPEB irradiation, the sample is composed of the lamellar pearlite and coarse ferrite. Figure 2(b)–(d) presents the surface morphologies of HCPEB-alloyed samples prepared with 10, 20, and 30 pulses, respectively. It can be seen that volcano-like craters were formed on the irradiated surface while the precoated Cr film disappeared. This result suggests that the surface was remelted after HCPEB alloying treatment, which resulted in the redistribution of elements that were uniformly dispersed in the material [27]. As the number of pulses increased, the crater density was gradually decreased. The volcano-like craters were formed due to the non-homogeneous local melting, and subsequent eruptions occurred near the subsurface when the matrix reached the melting point. Many previous studies have shown that the inclusions and second phases on the surface were more likely acted as nucleation sites for crater eruption [28–30]. The crater density was decreased with the number of pulses due to the gradual eruption of the inclusions, which could bring about a significant effect, the so-called "selective purification" effect [28, 31]. This effect is crucial for improving the corrosion resistance of the materials.

Figure 3(a) and (b) shows the representative SEM images of the surface of HCPEB samples alloys with 20 and 30 pulses, respectively. Obviously, the surface was remelted, and the precoated Cr powders completely disappeared on the irradiated surface of the samples alloys. As seen in Figure 3(a), the crater had a deep center-dimpling shape with a small bottom hole (marked with a red arrow), which confirmed the melting and eruption of local subsurface layer. After 30-pulsed HCPEB irradiation (Figure 3(b)), the number of craters was decreased visibly, whereas the depth was shallow. In other words, the surface became smoother, which is consistent with the results obtained by light microscopy. Besides, the EDS analysis (inset in Figure 3(b)) indicates that the surface is rich in Cr after HCPEB alloying. The Cr-rich solid solution in the steel will have a crucial role in improving the surface strength and corrosion resistance of the

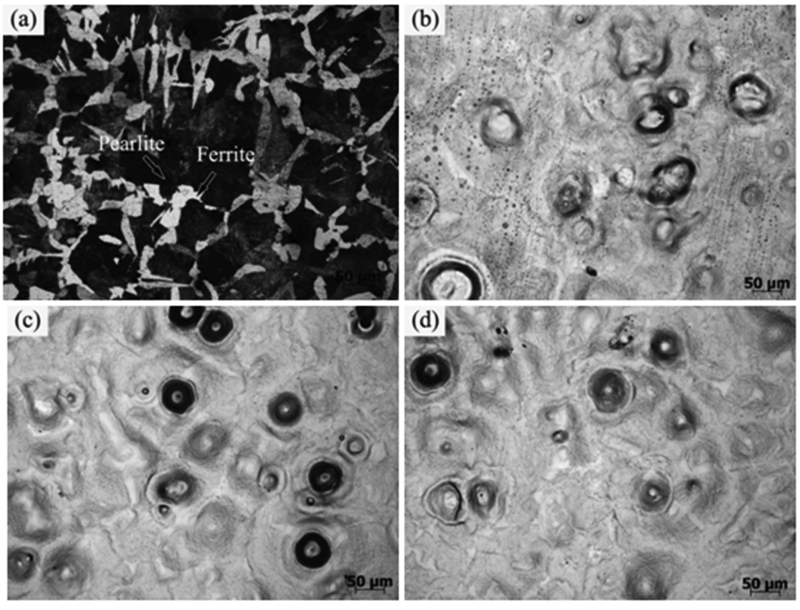


**Figure 2:** Metallographic morphologies of medium carbon steel before and after HCPEB alloying treatment. (a) initial, (b) 10, (c) 20, and (d) 30 pulses.

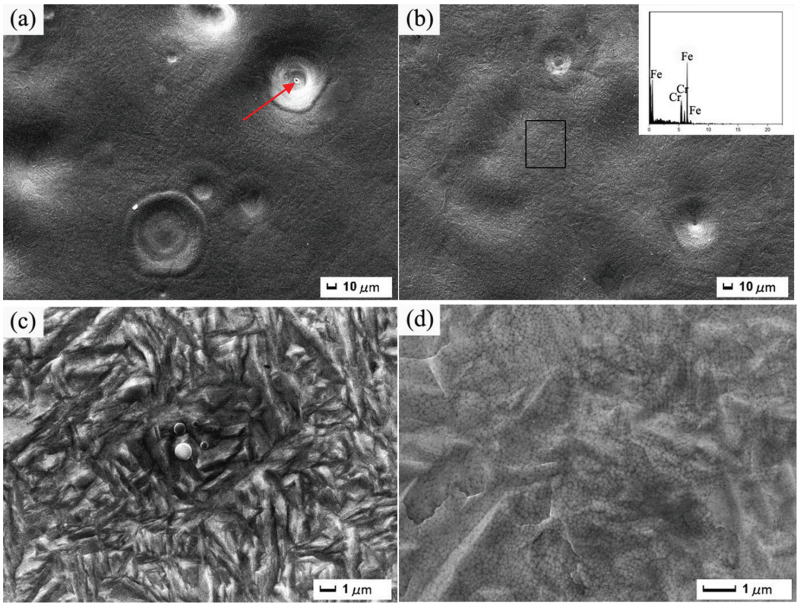


**Figure 3:** Surface SEM images of the alloyed samples. (a) and (c) 20 pulses, (b) and (d) 30 pulses.

material [32, 33]. High resolution SEM images of samples alloys are given in Figure 3(c) and (d). One can see that, in addition to the typical morphology, two other visible features can be also obtained on the alloying surface. The first one is associated with the formation of martensitic structures in some areas of 20-pulsed sample alloy (Figure 3(c)), which was caused by the rapid heating and cooling processes. Another one was related to the nano-structures i. e. refined austenite grains, which are generated on the alloying surface after 30-pulsed HCPEB irradiation due to the "self-cooling hardening" effect. Extremely fast solidification and cooling processes favor the formation of large numbers of nucleus, which do not have enough time to grow. Consequently, the nanoscale grains were formed on the irradiated surface. It is evident that the phase transformation occurred after HCPEB alloying. The formation of these nano grains is defining for the global properties of the material surface, which will be improved [34].

In Figure 4, the cross-sectional SEM images of the samples after HCPEB alloying treatment with different pulses are displayed. As noticed, an alloyed layer was formed on the top surface, which was obviously different from the substrate. The modified surface exhibits a stratified structure composed of a remelted layer, a heat affected zone, and a substrate matrix. The corresponding thickness of this mixed alloy layer increased with the increasing of the number of HCPEB pulses, and it was about 4–9 μm (Figure 4(a)–(c)). Punctual EDS analysis on the image in Figure 4(c) shows that the content of Cr element in the remelted layer was much higher than that of the substrate, which was about 8 μm length (Figure 4 (d)). This result sustains the formation of the Cr-rich alloyed layer after HCPEB alloying.

Figure 5(a)-(c) shows the TEM bright field images of the irradiated samples with 20 pulses. Figure 5(a) reveals that the lath-like martensitic structures were formed in certain regions of the irradiated layer while Figure 5(b) shows the dislocation cells in ferrite, which was a typical structure of the strongly textured metal material formed by the entanglement of the high density of dislocations. The dislocation needed a rearrangement to reduce energy while the entanglement of dislocation prevented the further dislocation slip. The dislocation subgrains were formed because of its lower energy [35]. Besides, there were many particles with an average size of about 0.24 μm found in the alloying layer (Figure 5(c)), which can be identified as $Cr_{23}C_6$ based on the corresponding selected area electron diffraction (SAED). Figure 5(d)–(f) shows the TEM images of the 30-pulsed alloyed sample. The grains with average sizes of about 186 nm were clearly observed (Figure 5(d)), which can be considered as austenite grains according to the result provided by SAED. This result is in good agreement with the SEM result illustrated in Figure 3. The micro-twinning was formed on the alloying surface as shown in Figure 5(c), revealing that the twinning deformation occurred after HCPEB irradiation. The micro-twinning consisted of a rapid and strongly deformation, which indicates that the HCPEB irradiation caused a severe plastic deformation [36], followed by the appearance of deformed structures, such as twins and complicated dislocation configurations. The diffusion of

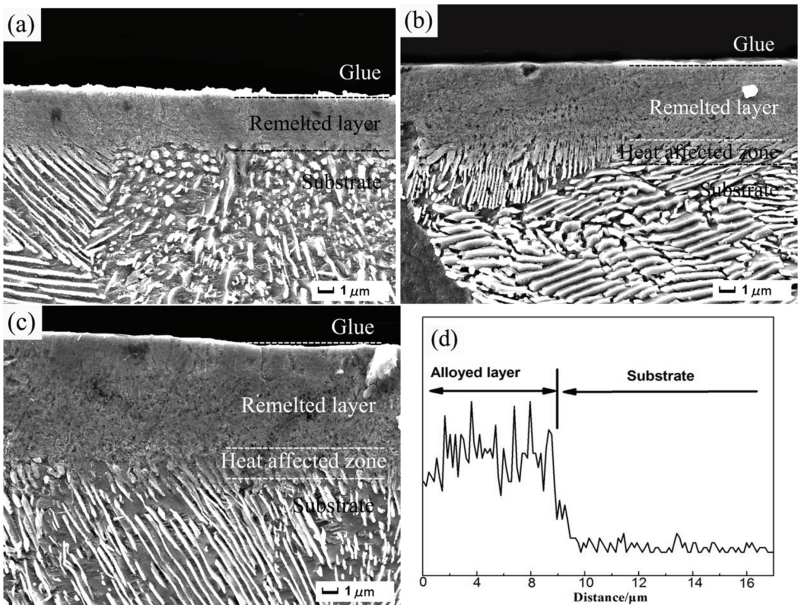


**Figure 4:** Cross-sectional SEM images of the alloying samples. (a) 10, (b) 20, (c) 30 pulses, and (d) the EDS line scanning of the alloying sample after 30 pulses.

Cr element can be promoted by these structures, whereas the grain boundaries of nano-crystalline structures are generated by a rapid solidification. Finally, a thick and compact alloying layer was formed. It was believed that the ultrafine grain size and dense solution of alloying elements in the austenite phase would inhibit the natural transformation of martensite. Thus, the degree of carbon alloying is a key factor for the stabilization of the austenite crystalline phase [37]. In Figure 5(f), Cr-rich carbides with smaller average size of about 10 nm were also formed in the alloying layer. These Cr-rich carbides can effectively prevent the movement of dislocation and subgrain boundaries improving the material strength by the effect of dispersion strengthening. In addition, the formation of the refined carbides is crucial for the austenite stabilization. Moreover, these carbides can improve the thermal fatigue properties of the material, as well [38, 39].

## Microhardness testing

Figure 6 illustrates the surface microhardness of the samples before and after HCPEB surface alloying after 10, 20, and 30 pulses. Compared with the original one (0 pulses), the surface microhardness of the irradiated samples was significantly increased as the number of pulses increased. The value of surface microhardness of 30-pulsed sample was the highest, which reached to 726 HV (about four times of the original one). It can be noticed that the sample prepared with 20 pulses displays a surface microhardness very close to that of the sample irradiated with 30 pulses. On this finding, it could be affirmed that an irradiation with 20 pulses could be as optimum to obtain a material with enhanced microhardenss. However, the results of the morphology and corrosion resistance clearly indicated that the 30-pulse sample shows improved properties reinforcing the idea that a number of 30 pulses is needed to provide a high performance alloyed material. After HCPEB irradiation, the modified layer surface of the medium carbon steel was transformed in a complex microstructure composed of martensite with very refined austenite phase. Besides, as the HCPEB pulses increases, the alloying element is better incorporated into the carbon lattice, which promotes the formation of Cr-rich carbides. These strengthening mechanisms, including martensitic hardening, fine grain strengthening, and solid solution strengthening are very important to improve the hardness of surface alloying layer by HCPEB treatment.

## Corrosion resistance testing

The polarization curves of the medium carbon steel in 3.5 wt. % NaCl solution before and after HCPEB alloying are displayed in Figure 7. The corrosion potential ($E_{corr}$) and corrosion current ($I_{corr}$) density measured by Tafel extrapolation are listed in Table 1. The $E_{corr}$ of alloyed samples was higher than that of the initial one, and the maximum value of −0.854 V was found after 30-pulsed

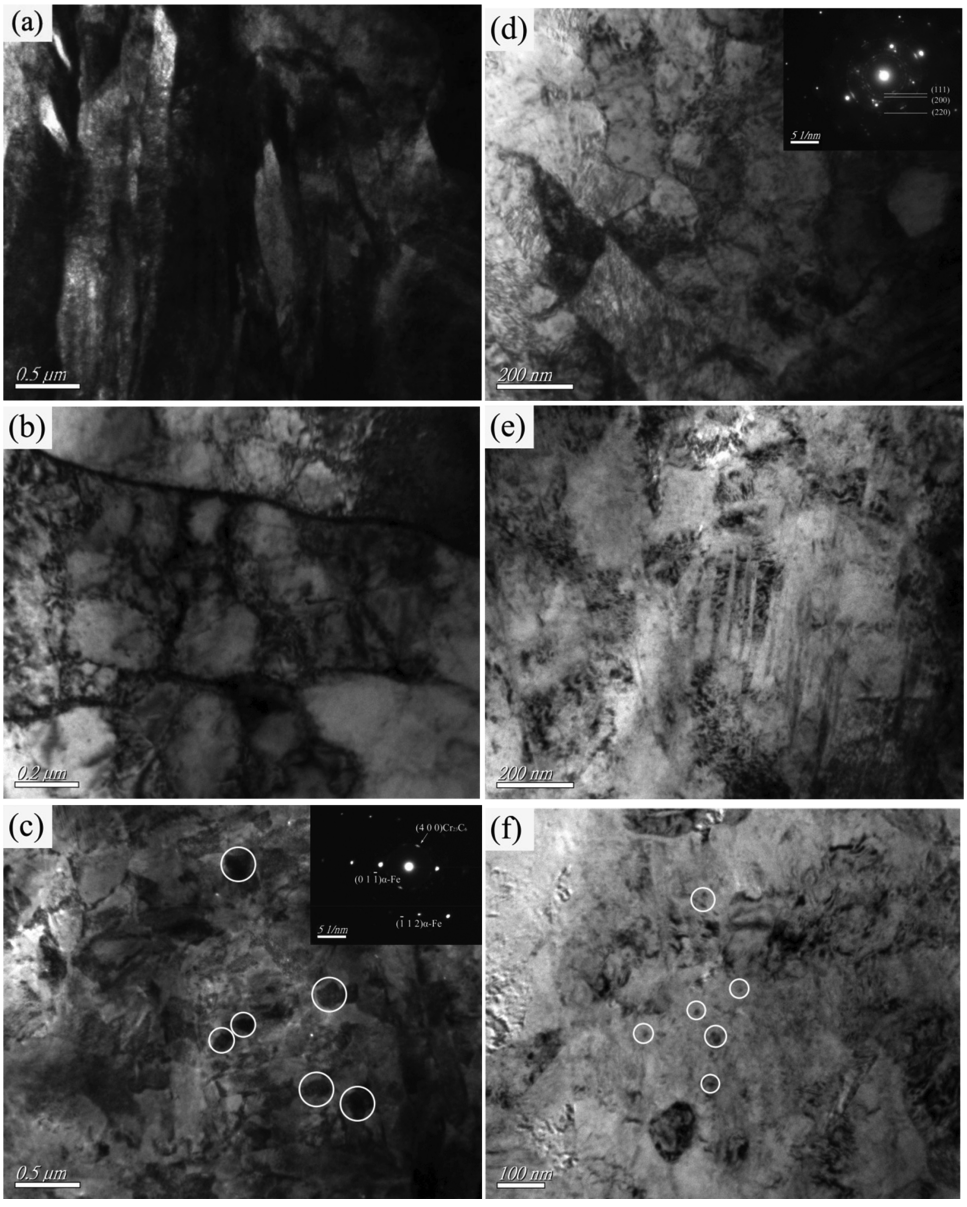


**Figure 5:** TEM images of medium carbon steel after HCPEB alloying with 20 pulses (a), (b), and (c) as well as 30 pulses (d), (e), and (f).

irradiation. Besides, the $I_{corr}$ density was decreased gradually after HCPEB surface alloying. The corrosion potential reflects the trend and thermodynamics of the reactions occurring on the alloyed surface while the corrosion current reflects the dynamics of corrosion, which is proportional to the rate of corrosion. The results showed that the corrosion resistance of the samples is improved significantly after HCPEB alloying treatment. The enhanced corrosion resistance was attributed to several factors, as follows. First, the presence of second phases or inclusions was prone to act as sites of corrosion pitting. The undesirable inclusions were erupted or dissolved due to the formation of craters induced by HCPEB irradiation, which is known as selective purification effect. Therefore, the reduction of corrosion pitting density can stimulate the formation of a smooth and denser protective oxide film. Secondly, the content of Cr in the alloying layer obtained by irradiation was much higher than that of the initial one. The Cr was highly reactive, which allowed the formation of the passive films on the surface. Therefore, the increased Cr content was essential to improve the corrosion resistance. Thirdly, the defect structures, such as grain boundaries, subgrain boundaries, and dislocations were formed, which can provide numerous channels by which Cr can

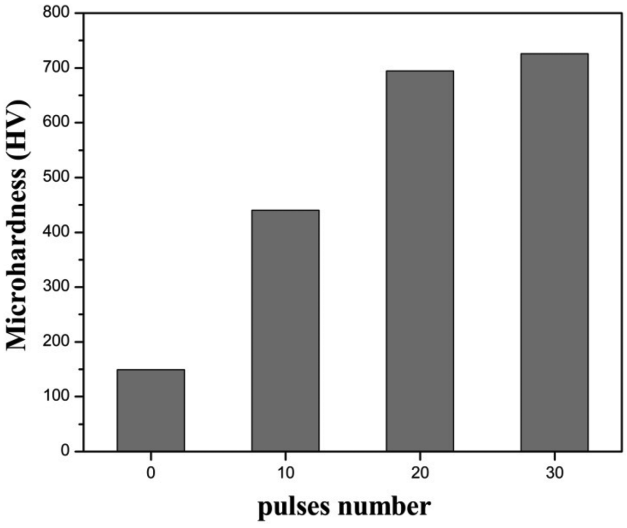


**Figure 6:** The surface microhardness of medium carbon steel before and after HCPEB alloying.

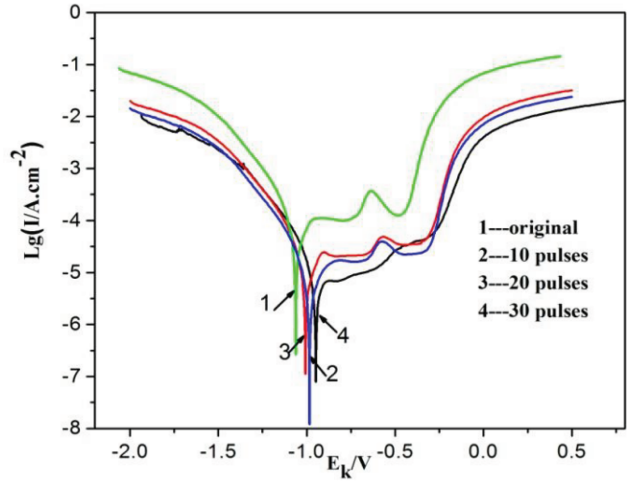


**Figure 7:** Polarization curve of medium carbon steel before and after HCPEB alloying.

**Table 1:** Electrochemical corrosion performance measurement.

| Samples | $I_{corr}$/μA·cm$^{-2}$ | $E_{corr}$/V |
|---|---|---|
| Initial | 88.03 | −1.252 |
| 10 pulses | 37.64 | −0.999 |
| 20 pulses | 42.27 | −1.008 |
| 30 pulses | 25.93 | −0.854 |

diffuse and form the protective film. Hence, a thick and dense chromium oxidation film (passive film) on the surface can be easily formed and it plays a noteworthy role in surface passivation. However, there are some differences regarding the corrosion resistance from a sample to another depending on the number of pulses. These differences are related to the formation of craters. As shown in Figure 2, for 10- and 20-pulsed samples, the numerous craters can hinder the formation of a continuous and dense protective passive film, which is detrimental for the corrosion resistance. The crater density of 30-pulsed sample was rather lower compared to that of other samples, which was reflected by the formation of a thicker, denser, and more stable passive layer. Under these above-mentioned factors, the corrosion resistance of the 30-pulsed sample was greatly improved.

## Conclusion

In conclusion, a systematic study on the surface chromium alloying processing of 0.45 C carbon steel by HCPEB experiments was performed. The main findings are summarized, as follows.

(1) After HCPEB alloying treatment, the thickness of the remelted layer, composed of lath martensite and ferrite, was about 4–9 μm. The Cr element diffused on the surface, and particles of tiny $Cr_{23}C_6$ were formed in the substrate.

(2) The surface microhardness of the material increased after HCPEB irradiation, and a dependence of the microhardness on the number of the irradiated pulses was noticed.

(3) The HCPEB alloying treatment significantly improved the corrosion resistance of the medium carbon steel. The solid solution, surface cleaning effect, and formation of nano-crystals in the alloying layer greatly improved the corrosion resistance of the materials.

**Acknowledgements:** This work was supported by the National Natural Sciences Foundation of China (Nos. 51601071, 51601072), Jiangsu Province Natural Science Foundation for Youths (No. BK20160530) and Youth Talent Development Program of Jiangsu University.

## References

[1] M. Szkodo, Surf. Coat. Tech., 296 (2016) 117–123.
[2] P. Xue, W.D. Li and D. Wang, Mater. Sci. Eng. A, 670 (2016) 153–158.
[3] S. Kumar, A. Bhattacharyya and D.K. Mondal, Wear, 270 (5–6) (2011) 413–421.
[4] N. Liu, Sci. Technol. Association Forum, 8 (2009) 69–70.
[5] S.X. Liu, Y. Chen, G.Q. Liu, X.F. Liu, Y.G. Zhang and J.K. Huang, Mater. Sci. Eng. A, 499 (1-2) (2009) 83–87.

[6] J.C. Oh, D.K. Choo and S. Lee, Surf. Coat. Tech., 127 (1) (2000) 76–85.
[7] K.V. Acker, D. Vanhoyweghen, R. Persoons and J. Vangrunderbeek, Wear, 258 (1–4) (2005) 194–202.
[8] X.W. Qiu, J. Netshape Forming Eng., 7 (3) (2015) 58–61.
[9] Y.H. Zhang and H. Zhang, Hot Working Tech., 4 (2000) 6–8.
[10] R.G. Davies, Metall. Trans. A, 9 (5) (1978) 671–679.
[11] M. Moonesan, A.H. Raouf and F. Madah, J. Alloy Compd., 520 (4) (2012) 226–231.
[12] L. Qin and C. Liu, Mater. Lett., 82 (2012) 127–129.
[13] P.Z. Zhang, Z. Xu and G.H. Zhang, Trans. Nonferrous Met. Soc. China, 16 (s3) (2006) 2100–2103.
[14] D. Chen, X. Dong and Z. Fan, China Foundry, 7 (1) (2010) 13–18.
[15] J. Zhu, M. Xu and W. Yang, Coatings, 7 (11) (2017) 191.
[16] Y. Chi, G. Gu and H. Yu, Opt. Laser Eng., 100 (2018) 23–37.
[17] M. Ansari, M.H. Sohi and R. Soltani, Int. J. Adv. Manuf. Tech., 83 (1-4) (2016) 285–291.
[18] A. Almeida and R. Vilar, Scr. Mater., 63 (8) (2010) 811–814.
[19] J. Cai, P. Lv, Q.F. Guan and A.C.S. Appl, Mater. Interfaces, 8 (2016) 32541–32556.
[20] C. Dong, A. Wu and S. Hao, Surf. Coat. Tech., 163-164 (2) (2003) 620–624.
[21] Q.F. Guan, H. Zou and G.T. Zou, Surf. Coat. Tech., 196 (1–3) (2005) 145–149.
[22] Y. Qin, A.M. Wu and J.X. Zou, High Power Laser Part. Beams, 15 (7) (2003) 701–704.
[23] Y. Qin, X.G. Wang, C. Dong and A. Phys, Sin., 52 (12) (2003) 3043–3048.
[24] J. Zou, Y. Qin and A. Wu, Nucl. Tech., 27 (7) (2004) 519–524.
[25] S.Z. Hao, D.Y. He and M.C. Li, Mater. Sci. Forum. Trans. Tech. Publ., 675 (2011) 1205–1208.
[26] C.S. Liu, S.Y. Chen and L.J. Shang, Chinese Journal of Lasers, 29 (3) (2002) 277–280.
[27] Q.F. Guan, G.T. Zhou and J. Lin, Jilin University.
[28] J. Zou, K. Zhang and C. Dong, Appl. Phys. Lett., 89 (4) (2006) 041913.
[29] C. Zhang, J. Cai, P. Lv, Y. Zhang, H. Xia and Q. Guan, J. Alloy Compd., 697 (2016) 69–103.
[30] C. Zhang, P. Lv, J. Cai, C.T. Peng, Y. Jin and Q. Guan, Appl. Surf. Sci., 422 (2017) 582–590.
[31] K.M. Zhang, J.X. Zou, T. Grosdidier, C. Dong and D. Yang, Surf. Coat. Tech., 201 (3–4) (2006) 1393–1400.
[32] L. Xu, B. Wang and J. Zhu, Appl. Sur. Sci., 379 (2016) 39–46.
[33] S. Jiang, F. Chai and H. Su, Corros. Sci., 123 (2017) 217–227.
[34] J. Zou, T. Grosdidier and K. Zhang, Acta Mater., 54 (20) (2006) 5409–5419.
[35] Q.F. Guan, D.Q. Cheng and D.H. Qiu, Acta Phys. Sin., 58 (7) (2009) 4846–4852.
[36] Q.F. Guan, Q. Zhang and C. Dong, Isij Int., 48 (2) (2008) 235–239.
[37] S. Hao, H. Wang and L. Zhao, Nucl. Instrum. Meth. Phys. Res. B, 368 (2016) 81–85.
[38] H. Wang, W. Yan and S.V. Zwaag, Acta Mater., 134 (2017) 143–154.
[39] K. Fukaura, Y. Yokoyama and D. Yokoi, Metall. Mater. Trans. A, 35 (4) (2004) 1289–1300.